Proceedings of the Canadian Society for Mechanical Engineering International Congress
32nd Annual Conference of the Computational Fluid Dynamics Society of Canada
Canadian Society of Rheology Symposium
CSME-CFDSC-CSR 2025
May 25–28, 2025, Montréal, Québec, Canada

Material Extrusion Additive Manufacturing of Aluminum-based Feedstocks

Gabriel Marcil-St-Onge[1a], Abdelberi Chandoul[1b], Yannig Thomas[2c], Roger Pelletier[2d], Louis-Philippe Lefebvre[2e] Vincent Demers[1f]

[1]Department of mechanical engineering, École de technologie supérieure, Montréal, QC, Canada
[2]National Research Council of Canada, Boucherville, QC, Canada
[a]gabriel.marcil-st-onge@etsmtl.ca
[b]abdelberi.chandoul.1@ens.etsmtl.ca
[c]Yannig.Thomas@cnrc-nrc.gc.ca
[d]Roger.Pelletier@cnrc-nrc.gc.ca
[e]Louis-Philippe.Lefebvre@cnrc-nrc.gc.ca
[f]vincent.demers@etsmtl.ca

Abstract—Aluminum and its alloys are widely used in industrial fields such as aerospace and automotive due to their excellent strength-to-weight ratio. However, the oxide layer that forms on the surface of aluminum poses challenges for powder metallurgy processes, particularly during sintering. Material extrusion, a powder-binder-based additive manufacturing process, is commonly employed for its simplicity and low cost, but remains largely unexplored for aluminum applications. This study investigates each step of the material extrusion process for aluminum. Feedstocks formulated with 65 vol. % AlSi10Mg powder, 25 vol. % paraffin wax, 2 vol. % stearic acid and 8 vol. % ethylene-vinyl acetate were used to print simple geometries. It was established that controlling the particle size distribution of the AlSi10Mg powder is critical for achieving good printability, where a powder blend containing both fine and coarse particles was required, enabling the feedstock to print hollow squares with minimal defects. The printed parts underwent thermal wick debinding at 250°C for 2 hours, successfully removing the majority of the binder. Loose powder and debound hollow squares were subsequently liquid-phase sintered at 575°C for 2 hours in a nitrogen atmosphere using sacrificial magnesium pellets as an oxygen getter. The sintered powders achieved an apparent density of 98%, while the hollow squares exhibited an adequate metallurgical continuity, but further development is required to address warping issues.

Keywords: Additive manufacturing, AlSi10Mg, material extrusion, debinding, sintering

I. Introduction

Additive manufacturing (AM), a group of seven layer-by-layer manufacturing processes, has experienced substantial growth in the last decade [1]. Among these, material extrusion (MEX), also known as fused deposition modeling (FDM), involves the creation of parts by extruding a filament of molten material through a heated nozzle onto a build platform. As the material cools down, it hardens, forming a foundation for subsequent layers. While MEX is widely recognized for its application in polymer-based rapid prototyping, the past decade has seen significant advancements that have expanded its range of printable materials.

In recent years, MEX has been adapted for manufacturing functional metallic or ceramic parts for aerospace, automotive, and medical industries [2-5]. This adaptation draws heavily from conventional powder injection molding (PIM), a process in which powder is mixed with polymer binders to formulate a feedstock. The feedstock is heated to a molten state and injected into a mold cavity, before cooling down and solidifying into the desired shape. The polymer binder is then removed through a debinding process, and the part is finally sintered to achieve the desired density [6]. Fundamentally, MEX replaces the molding step with a 3D printing step, offering the significant advantage of eliminating the need for molds, thereby drastically reducing equipment costs. However, MEX also introduces unique challenges. Because the raw material is in powder form, it must be sinterable. For metallic MEX, the range of usable alloys is expected to align closely with those commonly used in metal injection molding (MIM). As a result, some of the most frequently studied metals in MEX include stainless steels (17-4PH and 316L) and titanium alloys (e.g., Ti-6Al-4V) for their excellent mechanical properties, as well as copper for its superior thermal and electrical conductivity [7].

This project was funded by the National Research Council of Canada (National Program Office, proposal #AM-125-1) and the Centre Québécois de Recherche et de Développement de l'Aluminium (project #1148).

Aluminum and its alloys are widely studied for their excellent strength-to-weight ratio, making them particularly valuable in the aerospace industry. However in powder metallurgy aluminum presents challenges due to the oxide layer that forms on the surface of the particles, which hinders interparticle bonding during sintering processes [8]. Despite these drawbacks, AM of aluminum alloys remains highly attractive due to the inherent advantages of AM technologies. Currently, AM of aluminum alloys is predominantly conducted using laser powder bed fusion (LPBF), with a focus on cast Al-Si alloys, such as AlSi7Mg, AlSi10Mg, and AlSi12 [9-11]. Conversely, the application of aluminum and its alloys in MEX remains weakly explored. Since the surge in MEX research and development, which began around 2015, only a handful of studies have addressed binder-based MEX of aluminum alloys [12-15]. In 2023, researchers attempted to print simple and complex geometries using AlSi10Mg MIM-like feedstocks [16] with a custom-built, plunger-based printer [17]. While efforts were made to optimize the viscosity of the feedstock by adjusting the percentage of thickener, the results indicated that the feedstocks were too sticky for effective printing. In this study, an alternative optimization approach for AlSi10Mg MEX feedstocks was proposed. Instead of focusing solely on viscosity adjustments, the effect of the particle size distribution (PSD) of the aluminum powder in the feedstock was investigated. Furthermore, the debinding and sintering processes are analyzed using simple printed geometries to better understand the feasibility of producing high-quality aluminum parts via MEX.

II. Methodology

A. Feedstock constituents and formulation

Three plasma-atomized AlSi10Mg powders with different PSD were studied: a typical MIM-grade powder (0-20 µm), a typical binder jetting powder (20-63 µm), and a mixed powder (0-110 µm). The powders were observed using a TM3000 Hitachi scanning electron microscope. As shown in Fig. 1, the three powder lots exhibit of near-perfectly spherical particles. The PSD plotted in Fig. 2 was measured using the dry powder system of a LS 13320 Backman Coulter laser diffraction particle size analyzer. The diameter percentiles D_{10}, D_{50} and D_{90} for each powder are listed in Table I. Feedstocks were prepared by mixing the aluminum powders with a binder composed of paraffin wax (PW), stearic acid (SA), and ethylene-vinyl acetate (EVA) blended at 110°C under vacuum for 120 minutes until fully homogenized. All feedstocks contained 65% aluminum particles, 25% PW, 2% SA and 8% EVA by volumetric proportions (Table II). These proportions were taken from a previous study [16] as they maximize solid loading while maintaining adequate viscosity for 3D printing. Properties and information about the powders and binder constituents are summarized in Table III. The viscosity profiles of feedstocks were measured using an Instron SR20 capillary rheometer at 90°C with a 1 mm diameter, 40 mm long capillary (Fig. 3). Note that feedstock made with the powder 20-63 µm could not be measured due to occurrence of binder segregation during testing.

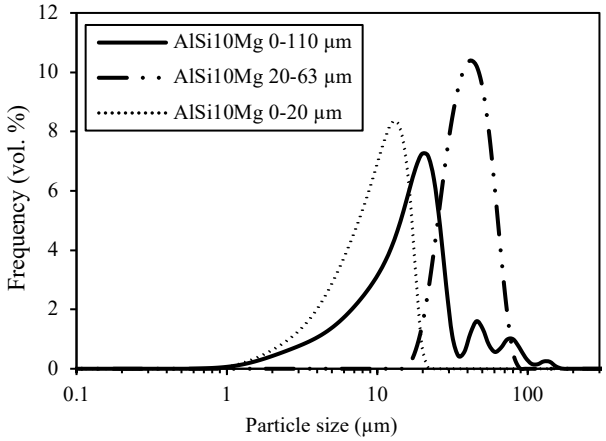

Figure 2. Particle size distribution of AlSi10Mg powders

B. Printing process

The parts were manufactured using a plunger-based 3D printer shown in Fig. 4 and described in [17]. This printer features a heated ram extruder that pushes molten feedstock through a fixed print head and extrudes it through a nozzle with a diameter of 0.4 mm. The build platform is capable of movement along all three axes and can be maintained at a constant temperature. Simple hollow squares were printed using a custom g-code file using the first-bead overlap (FBO) strategy, which was recently developed to eliminate interlayer rhomboid voids typically observed in MEX-printed parts, while

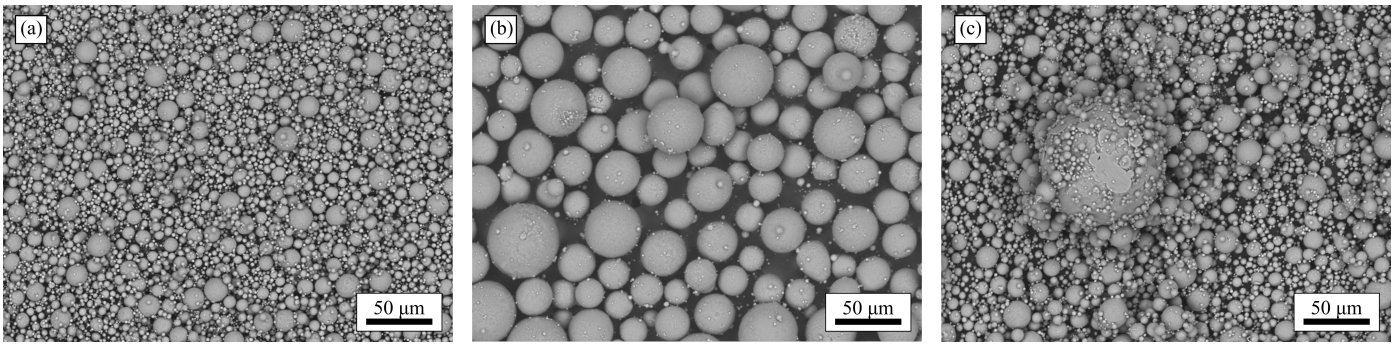

Figure 1. SEM micrographs of AlSi10Mg powders: (a) 0-20 µm, (b) 20-63 µm and (c) 0-110 µm

TABLE I. PARTICLE SIZE PERCENTILES OF ALUMINUM POWDERS

Powder	D_{10} (µm)	D_{50} (µm)	D_{90} (µm)
AlSi10Mg 0-20 µm	4	10	16
AlSi10Mg 20-63 µm	26	40	60
AlSi10Mg 0-110 µm	5	17	41

TABLE II. FEEDSTOCKS FORMULATIONS

Feedstocks	Constituents (vol. %)					
	Al 0-20 µm	*Al 20-63 µm*	*Al 0-110 µm*	*PW*	*SA*	*EVA*
Al 0-20	65	0	0	25	2	8
Al 20-63	0	65	0	25	2	8
Al 0-110	0	0	65	25	2	8

TABLE III. PROPERTIES OF THE FEEDSTOCK CONSTITUENTS

Constituents	Melting Point (°C)	Density (g/cm^3)	Supplier
AlSi10Mg 0-20 µm	550	2.65	AP&C
AlSi10Mg 20-63 µm	550	2.65	AP&C
AlSi10Mg 0-110 µm	550	2.65	AP&C
Paraffin wax (PW)	57	0.90	Sigma-Aldrich
Stearic acid (SA)	73	0.99	Sigma-Aldrich
Ethylene-vinyl acetate (EVA)	70	0.94	DuPont

also minimizing over-extrusion defects and dimensional inconsistencies [18]. The FBO technique overlaps at 35% only the first two beads of each layer. Additionally, a complex geometry was printed using g-code generated by Ultimaker Cura 4.8.0 slicer software without implementing the FBO technique. The following constant printing parameters were used for all parts: layer height (0.2 mm), bead width (0.4 mm), printing speed (20 mm/s), build platform temperature (50°C), and print head temperature (90°C).

C. Debinding and sintering processes

The green (as-printed) parts underwent debinding using a thermal wick debinding process. Printed specimens were placed on a bed of compressed fine submicron alumina powder inside a stainless steel container, which was then completely filled with alumina powder and compressed manually to ensure uniform packing. The container was placed in a furnace (H41/H Narbertherm) and subjected to a thermal treatment at 250°C for 2 hours under an industrial-grade argon atmosphere. After the debinding process, the parts were carefully excavated from the alumina powder bed and lightly brushed to remove any excess alumina particles adhering to their surfaces.

Sintering aluminum presents significant challenges due to the oxide layer that naturally forms on the surface of the particles. This oxide layer inhibits solid-state sintering [19], making liquid-state sintering the preferred method. The sintering process developed in this study was inspired by methods employing sacrificial magnesium blocks as oxygen getters to facilitate sintering [20, 21]. As shown in Fig. 5, control samples (loose AlSi10Mg powder in a stainless steel ring) and debound printed parts were placed on a stainless steel sintering tray and surrounded by magnesium pellets. The tray was then positioned in a furnace (Lindberg model 54579), where high-purity nitrogen gas was introduced for 60 minutes to remove the air and then maintained for the entire cycle. Nitrogen was selected as the sintering atmosphere due to its

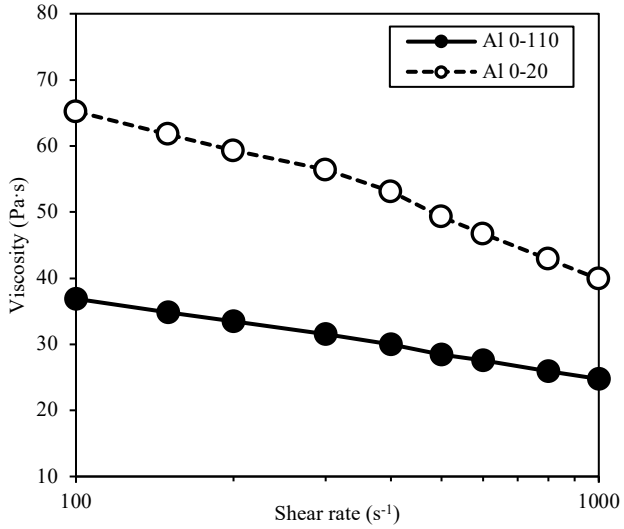

Figure 3. Viscosity of AlSi10Mg feedstocks

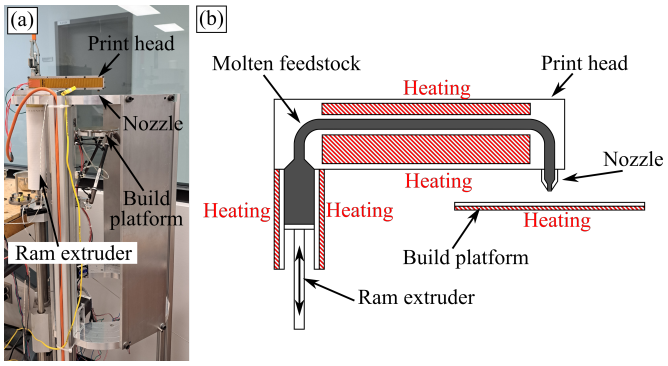

Figure 4. (a) 3D printer, and (b) schematic representation of the process

Figure 5. Sintering setup

ability to promote high densification and optimal mechanical properties in aluminum alloys [22, 23]. The furnace temperature was raised to 575°C and held for 2 hours. After sintering, the specimens were cut and polished before to be observed using a LEXT4100 laser confocal microscope.

III. Results and Discussion

A. *Effects of powder particle size distribution on the printability of MEX feedstocks*

Among the three feedstocks studied, only the Al 0-110 feedstock was successfully printable. An example of a hollow square printed using this feedstock is shown in Fig. 6a. The printed part maintained its expected dimensions, with only minor over-extrusion defects located at the starting points of new layers. The cross-sectional view reveals only two very small rhomboid voids (indicated by arrows in Fig. 6b) demonstrating that the FBO technique effectively filled these voids without compromising the overall quality of the part. This feedstock was also used to print a complex geometry (expected shape shown in Fig. 6c), but a too low feedstock viscosity negatively impacted the printing quality for this intricate design (Fig. 6d).

In a previous study [16], a feedstock similar to Al 0-20 (with the same aluminum powder PSD) was printed, but the parts exhibited over-extrusions along their perimeter. The Al 0-20 feedstock in this study demonstrated similar characteristics as described in [16]. It had a sticky or doughy consistency, deviating from the typical liquid-like behavior of MEX feedstocks. The higher viscosity of Al 0-20 compared to Al 0-110 could explain this difference in consistency. However, this behavior contrasts with the liquid-like consistency of commonly used stainless steel- based feedstocks [24], which possess similar or even higher viscosity profiles than Al 0-20. As presented in Fig. 7, the Al 0-20 feedstock printed approximately half of a hollow square before the nozzle clogged. Despite multiple attempts, no complete hollow square could be printed with the Al 0-20 feedstock.

The Al 20-63 feedstock was neither printable nor suitable for rheology testing due to binder segregation. These

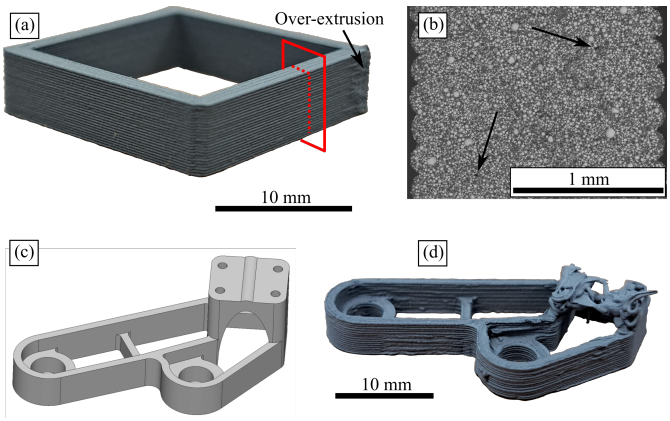

Figure 6. Printing of the Al 0-110 feedstock: (a) printed hollow square, (b) SEM observation of the cross-section of a hollow square, (c) STL representation and (d) printing of a complex geometry

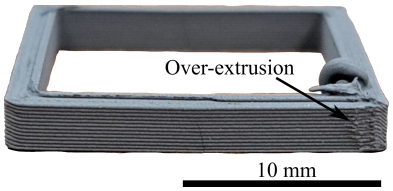

Figure 7. Interrupted printing of a hollow square printed with the Al 0-20 feedstock

observations suggest that fine particles seem required for preventing binder segregation, while coarser particles contribute to improved flowability and consistency. Therefore, a balanced combination of fine and coarse particles appears essential for achieving optimal performance in MEX feedstocks.

B. *Debinding and sintering of AlSi10Mg powders and printed parts*

Thermal wick debinding was performed on hollow squares printed with the Al 0-110 feedstock. The debound parts were brittle, but they could be handled with care and were easily retrieved from the alumina wicking medium. Fig. 8 presents micrographs captured at the center of a cross-section of a printed square, both before and after the debinding process. The binder maintaining particles initially (Fig. 8a) was successfully almost completely drawn out of the part (Fig. 8b).

The sintering cycle was initially tested on loose AlSi10Mg powders, including the 0-20 µm and 20-63 µm powders, even though both were not printable. Fig. 9 presents images of the powder samples and their respective micrographs. The visual appearance of the compacts is similar across all samples. The micrographs reveal a sintered microstructure, where some particles are still clearly visible with their very spherical shape, while others have melted, and thus contributing to the metallurgical continuity of the parts. The dark gray regions are the Si-rich phases. For the 20-63 µm and 0-110 µm powders (Fig. 9b and c, respectively), few pores are visible. The relative density of these sintered powder samples was measured to be between 97 and 98% using Archimedes' principle as per ASTM B962-23 standard [25]. Several factors contributed to achieving this result. As mentioned earlier, sacrificial magnesium pellets were used as oxygen getters because of their higher affinity for oxygen than aluminum. These pellets prevented the formation of aluminum oxide on the outer layers of the samples during

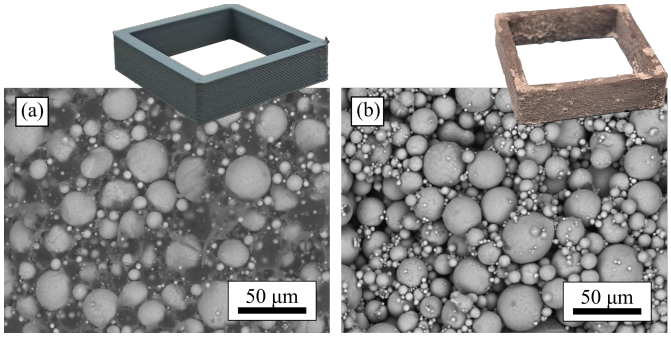

Figure 8. Photos and micrographs of cross-sections of a printed part (a) before and (b) after debinding

sintering [21]. The pure nitrogen atmosphere reacted with the aluminum to form aluminum nitride and promote pore filling [23]. Finally, the magnesium alloying element in AlSi10Mg is known to migrate at the surface of the particles during sintering, breaking down the oxide layer and facilitating sintering [26, 27].

The high occurrence of porosities obtained with the 0-20 µm powder (Fig. 9a) confirms a weak sinterability of this powder. A deeper investigation is thus required to identify the root cause of this unexpected result.

After confirming the sintering cycle on powder samples, it was also tested on debound Al 0-110 hollow squares. Fig. 10 presents photos of squares sintered at different temperatures, along with micrographs of their cross-sections. In Fig. 10a, it can be seen that the sintering cycle at 575°C produced a microstructure similar to that of the powder sample, but the hollow square was warped and cracked. Warping typically occurs due to non-uniform stresses, especially during the cooling phase of sintering and with thin parts. However, rather than optimizing the cooling phase, the effect of lowering the sintering temperature was explored. Fig. 10b shows that even with a 5°C reduction, the square displays minimal warping, but the microstructure appears slightly different (with smaller Si-rich phases), and porosity is increasing. These observations become more pronounced in Fig. 10c and d, where the decreased warping and increased porosity are more evident at 10°C and 20°C lower sintering temperatures, respectively. These findings indicate that the sintering cycle is currently non-optimal for printed parts and needs to be investigated in the future.

IV. Conclusions

In this study, the complete process of manufacturing AlSi10Mg parts via MEX was investigated. Low-viscosity feedstocks, containing 25 vol.% PW, 2 vol.% SA, 8 vol.% EVA, and 65 vol.% solid loading with varying PSDs, were tested. It was found that using a blend of both fine and coarse aluminum particles was optimal for printing; however, further investigation into the feedstock's viscosity is needed for printing complex geometries. Printed hollow squares were debound using a thermal wick process with submicron alumina as the wicking medium (250°C for 2 hours). Liquid-phase sintering (575°C for 2 hours) was carried out on powder samples and debound hollow squares. The use of magnesium and a nitrogen atmosphere were keys for the sintering of AlSi10Mg. This study confirmed that it is possible to print via MEX process, debind, and sinter aluminum powder to produce an adequate metallurgical continuity. However, the warping issue suggests that the sintering process needs to be optimized.

Acknowledgements

The authors would like to thank the CNRC R&D industrial consortium METALTec for initiating this project, with special thanks to the industrial partners AP&C and Dana Incorporated for their active participation in the project.

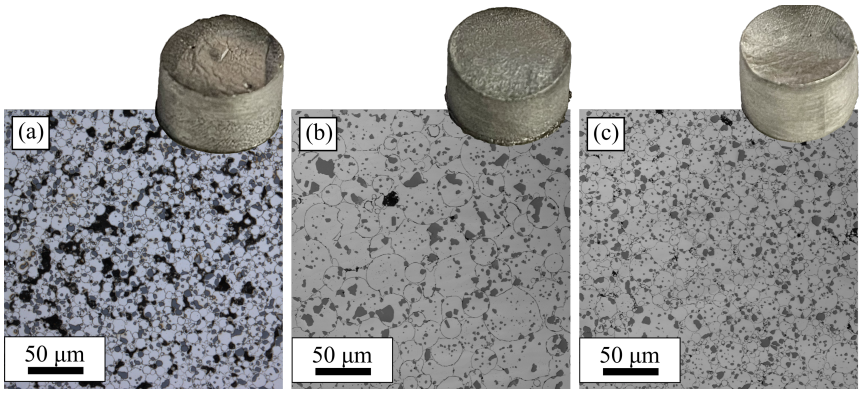

Figure 9. Photos and micrographs of sintered powder samples: (a) 0-20 µm, (b) 20-63 µm and (c) 0-110 µm

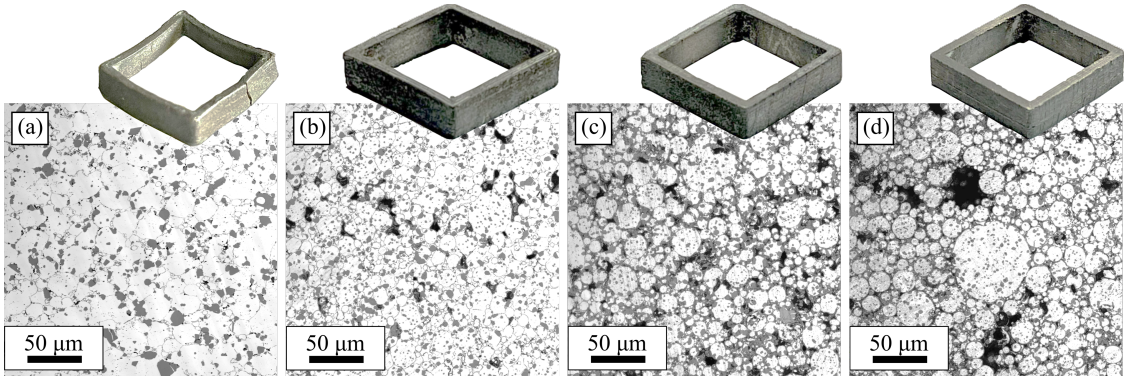

Figure 10. Photos and micrographs of Al 0-110 sintered hollow squares at (a) 575°C, (b) 570°C, (c) 565°C and (d) 555°C

References

[1] *Additive manufacturing — General principles — Fundamentals and vocabulary*, 52900:2021, ISO/ASTM, 2021. [Online]. Available: https://www.iso.org/obp/ui/#iso:std:iso-astm:52900:ed-2:v1:en

[2] J. Xu, Y. Fei, Y. Zhu, W. Yu, D. Yao, and J. G. Zhou, "A review of non-powder-bed metal additive manufacturing: techniques and challenges," *Materials,* vol. 17, no. 19, p. 4717, 2024, doi: 10.3390/ma17194717.

[3] M. Sadaf, M. Bragaglia, L. Slemenik Perše, and F. Nanni, "Advancements in metal additive manufacturing: a comprehensive review of material extrusion with highly filled polymers," *Journal of Manufacturing and Materials Processing*, vol. 8, no. 1*,* doi: 10.3390/jmmp8010014.

[4] K. Rane and M. Strano, "A comprehensive review of extrusion-based additive manufacturing processes for rapid production of metallic and ceramic parts," *Advances in Manufacturing,* vol. 7, no. 2, pp. 155-173, 2019/06/01 2019, doi: 10.1007/s40436-019-00253-6.

[5] R. Spina and L. Morfini, "Material extrusion additive manufacturing of ceramics: a review on filament-based process," *Materials*, vol. 17, no. 11*,* doi: 10.3390/ma17112779.

[6] D. F. Heaney, *Handbook of metal injection molding*. Woodhead Publishing, 2019.

[7] C. Suwanpreecha and A. Manonukul, "A review on material extrusion additive manufacturing of metal and how it compares with metal injection moulding," *Metals,* vol. 12, no. 3, p. 429, 2022, doi: 10.3390/met12030429.

[8] S. S. Gutin, A. A. Panov, and M. I. Khlopin, "Effect of oxide films in the sintering of aluminum powders," *Soviet Powder Metallurgy and Metal Ceramics,* vol. 11, no. 4, pp. 280-282, 1972/04/01 1972, doi: 10.1007/BF00800343.

[9] Z. Zhu *et al.*, "Recent progress on the additive manufacturing of aluminum alloys and aluminum matrix composites: microstructure, properties, and applications," *International Journal of Machine Tools and Manufacture,* vol. 190, p. 104047, 2023/08/01/ 2023, doi: 10.1016/j.ijmachtools.2023.104047.

[10] P. A. Rometsch, Y. Zhu, X. Wu, and A. Huang, "Review of high-strength aluminium alloys for additive manufacturing by laser powder bed fusion," *Materials & Design,* vol. 219, p. 110779, 2022/07/01/ 2022, doi: 10.1016/j.matdes.2022.110779.

[11] N. T. Aboulkhair, M. Simonelli, L. Parry, I. Ashcroft, C. Tuck, and R. Hague, "3D printing of aluminium alloys: additive manufacturing of aluminium alloys using selective laser melting," *Progress in Materials Science,* vol. 106, p. 100578, 2019/12/01/ 2019, doi: 10.1016/j.pmatsci.2019.100578.

[12] S. Dayam, P. Tandon, and S. Priyadarshi, "Development of paste extrusion-based metal additive manufacturing process," *Rapid Prototyping Journal,* vol. 28, no. 10, pp. 1920-1932, 2022, doi: 10.1108/RPJ-05-2021-0118.

[13] S. Tang, Y. Yang, L. Yang, and Z. Fan, "A green extrusion-based 3D printing of hierarchically porous aluminum," *Powder Technology,* vol. 399, p. 117198, 2022/02/01/ 2022, doi: 10.1016/j.powtec.2022.117198.

[14] V. Momeni *et al.*, "Effects of different polypropylene (PP)-backbones in aluminium feedstock for fused filament fabrication (FFF)," *Polymers,* vol. 15, no. 14, p. 3007, 2023, doi: 10.3390/polym15143007.

[15] S. K.Manchili, G. Singh, J.-M. Missiaen, and D. Bouvard, "Additive manufacturing of aluminum Al 6061 alloy using metal injection molding granules: green density, surface roughness, and tomography study," *Progress in Additive Manufacturing,* 2024/09/13 2024, doi: 10.1007/s40964-024-00791-x.

[16] D. Delbergue, L. Boudeau, and V. Demers, "Development of an aluminum-based feedstock for material extrusion 3D printing," presented at the Advances in Additive Manufacturing with Powder Metallurgy, Las Vegas , NV, USA, 2023.

[17] O. Miclette, R. Côté, V. Demers, and V. Brailovski, "Material extrusion additive manufacturing of low-viscosity metallic feedstocks: performances of the plunger-based approach," *Additive Manufacturing,* vol. 60, p. 103252, 2022/12/01/ 2022, doi: 10.1016/j.addma.2022.103252.

[18] R. Côté, V. Demers, N. R. Demarquette, S. Charlon, and J. Soulestin, "A strategy to eliminate interbead defects and improve dimensional accuracy in material extrusion 3D printing of highly filled polymer," *Additive Manufacturing,* vol. 68, p. 103509, 2023/04/25/ 2023, doi: 10.1016/j.addma.2023.103509.

[19] R. Q. Guo, P. K. Rohatgi, and D. Nath, "Preparation of aluminium-fly ash particulate composite by powder metallurgy technique," *Journal of Materials Science,* vol. 32, no. 15, pp. 3971-3974, 1997/08/01 1997, doi: 10.1023/A:1018625118090.

[20] K. S. Yasuhiro Nakao, Shigehisa Seya, Takeshi Sakuma, "Process for producing aluminum sintering," United States Patent US5525292A, Jun. 11, 1996.

[21] Z. Y. Liu, T. B. Sercombe, and G. B. Schaffer, "Metal injection moulding of aluminium alloy 6061 with tin," *Powder Metallurgy,* vol. 51, no. 1, pp. 78-83, 2008, doi: 10.1179/174329008x284859.

[22] T. Pieczonka, T. Schubert, S. Baunack, and B. Kieback, "Sintering behaviour of aluminium in different atmospheres," in *Sintering*, 2005, pp. 331-334.

[23] G. B. Schaffer, B. J. Hall, S. J. Bonner, S. H. Huo, and T. B. Sercombe, "The effect of the atmosphere and the role of pore filling on the sintering of aluminium," *Acta Materialia,* vol. 54, no. 1, pp. 131-138, 2006/01/01 2006, doi: 10.1016/j.actamat.2005.08.032.

[24] M. A. Omrane, R. Côté, and V. Demers, "Optimization of the printability envelope of low-viscosity powder-binder feedstocks used in material extrusion 3D printing," *Rapid Prototyping Journal,* vol. 30, no. 2, pp. 364-377, 2024, doi: 10.1108/RPJ-08-2023-0266.

[25] *Standard Test Methods for Density of Compacted or Sintered Powder Metallurgy (PM) Products Using Archimedes' Principle*, B962 − 23, ASTM, 2023.

[26] R. N. Lumley, T. B. Sercombe, and G. M. Schaffer, "Surface oxide and the role of magnesium during the sintering of aluminum," *Metallurgical and Materials Transactions A,* vol. 30, no. 2, pp. 457-463, 1999/02/01 1999, doi: 10.1007/s11661-999-0335-y.

[27] G. B. Schaffer, T. B. Sercombe, and R. N. Lumley, "Liquid phase sintering of aluminium alloys," *Materials Chemistry and Physics,* vol. 67, no. 1, pp. 85-91, 2001/01/15 2001, doi: 10.1016/S0254-0584(00)00424-7.